Development of a Femtosecond Soft X-ray SASE FEL at DESY

W. Brefeld [a], B. Faatz [a], J. Feldhaus [a], M. Körfer [a],
J. Krzywinski [b], T. Möller [a], J. Pflueger [a], J. Rossbach [a],
E.L. Saldin [a], E.A. Schneidmiller [a], S. Schreiber [a], and
M.V. Yurkov [c]

[a] *Deutsches Elektronen-Synchrotron (DESY), Notkestrasse 85, D-22607 Hamburg, Germany*

[b] *Institute of Physics of the Polish Academy of Sciences, 02688 Warszawa, Poland*

[c] *Joint Institute for Nuclear Research, Dubna, 141980 Moscow Region, Russia*

Abstract

In this paper we describe the extension of the soft X-ray SASE FEL at the TESLA Test Facility (TTF) at DESY for generation of femtosecond pulses. The idea is based on a technique of "manipulating" the energy spread along the electron bunch. Since the radiation amplification process is extremely sensitive to the value of the energy spread, only that part of the electron bunch radiates which has low energy spread. A novel technique is proposed for preparation of electron beam with required shaping of the energy spread allowing to overcome the problem of electron pulse jitter (about ± 1 ps). The system consists of two undulators separated by electron bypass and optical pulse shaping system. Undulators are tuned for amplification of the radiation with 523 nm wavelength. A seed radiation pulse (10 ps pulse duration, 0.3 μJ pulse energy, 30 kW peak power) is generated by present TTF laser facility. The first undulator operates in the linear regime and produces 300 fs radiation pulse naturally synchronized with the electron bunch. After the exit of the first undulator the electron bunch is guided through a bypass, and the light enters the pulse shaping system. The shaping system produces zero area light pulse (i.e. the pulse with zero value of optical field in the central area of the pulse) which is amplified up to the saturation level in the second undulator. Large energy spread is induced in the significant fraction of the electron beam due to the FEL interaction process, and only a small part of the electron bunch (near the center of zero area light pulse) is capable to produce radiation in the 6 nm SASE FEL. The SASE FEL described in this paper will provide soft X-ray pulses with 30 fs (FWHM) duration. On the basis of the TTF parameters it should be possible to achieve an average brilliance of 10^{22} photons $\mathrm{s}^{-1}\mathrm{mrad}^{-2}\mathrm{mm}^{-2}$ per 0.1% BW. The average number of photons can exceed 10^{12} photon/pulse. Present conceptual design is compatible with the layout of the soft X-ray SASE FEL being under construction at DESY and can be realized with minimal additional efforts.

1 Introduction

Phase transitions, surface processes, and chemical reactions are ultimately driven by the motion of atoms on the time scale of one vibrational period ($\simeq$ 100 fs). Unfortunately, the pulse length of present synchrotron light sources is too long for resolving atomic motion on the 100 femtosecond time scale. Recent efforts at applying 300 fs X-rays pulses to probe structural dynamics have used a synchrotron source combined with a femtosecond optical quantum laser [1]. The same technique can be used to generate in the future 100 fs X-ray pulses with an average brilliance of 10^{11} photons $s^{-1}mrad^{-2}mm^{-2}$ per 0.1% BW at the photon energy of 2 keV [1].

Femtosecond soft X-ray facility proposed in this paper is based on the use of soft X-ray SASE FEL. To be specific, we illustrate a new method of femtosecond X-ray pulses production with an example for the SASE FEL at the TESLA Test Facility (TTF) being under construction at DESY. Practical goal of our study was also to design femtosecond facility which is compatible with the present design of the TTF and the soft X-ray SASE FEL, and which can be realized with minimal additional efforts.

The idea for production of very short X-ray pulses is based on a high sensitivity of the FEL gain on the energy spread in the electron beam. Thus, a technique best suited for the femtosecond SASE FEL consists of "manipulating" the energy spread along the electron bunch. The required shaping of the energy spread is performed by passing the electron beam trough two-stage FEL amplifier (see Fig. 1) seeded by an optical pulse from existent TTF laser facility (pulse duration 10 ps, optical energy in the pulse 0.3 μJ, wavelength 523 nm – the 2nd harmonic of Nd:YLF laser). The first stage of the FEL amplifier operates in the linear regime and produces optical pulses of 300 fs pulse duration with peak power of about 60 kW which is strictly synchronized with the electron bunch. After the exit of the first stage the electron bunch is guided through a bypass, and the radiation enters the pulse shaping system. The functions of the electron bypass are to provide equal time delays for the electron and the light beams, and to suppress microbunching induced in the electron bunch in the first undulator due to the FEL process. The function of the optical pulse shaping system is to prepare zero area optical pulse (see Fig. 2). In pulse shaping system the input radiation is focused into a single-mode optical fiber. After the fiber exit, the linear chirped pulse is sent through spectral filtering system. The pulse is spectrally dispersed using a grating and directed through a mask which spectrally filters the pulse. The spectral components are recollimated into a beam by a second grating. The shaping system produces zero area pulses which are strictly synchronized with electron bunches at the entrance to the second undulator. Since the input optical pulse is produced by the same electron bunch, the proposed scheme tolerates electron pulse time jitter of about a few picoseconds. A zero area op-
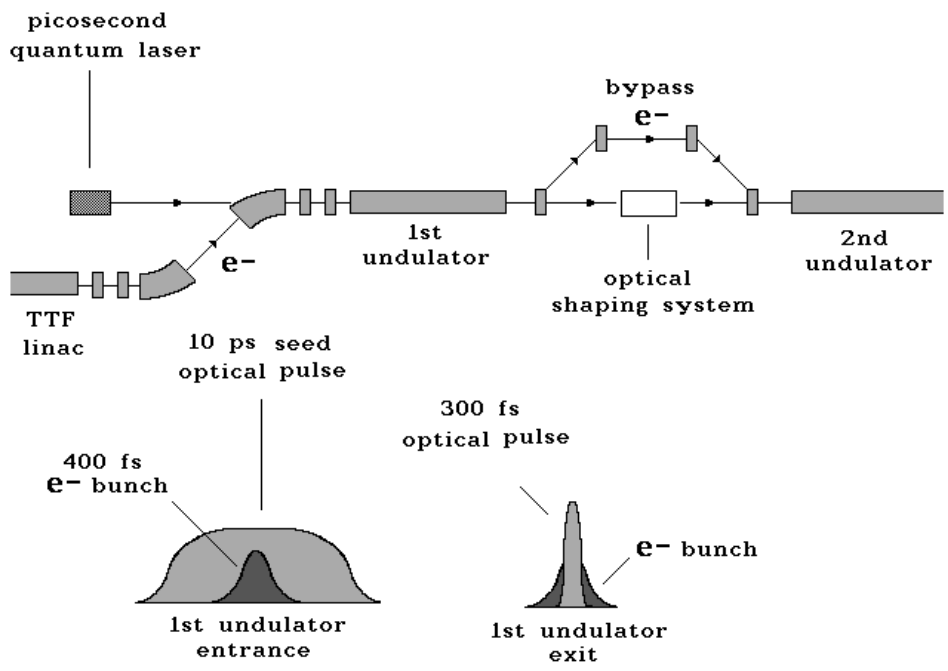
Fig. 1. The two stage scheme of the seeding system
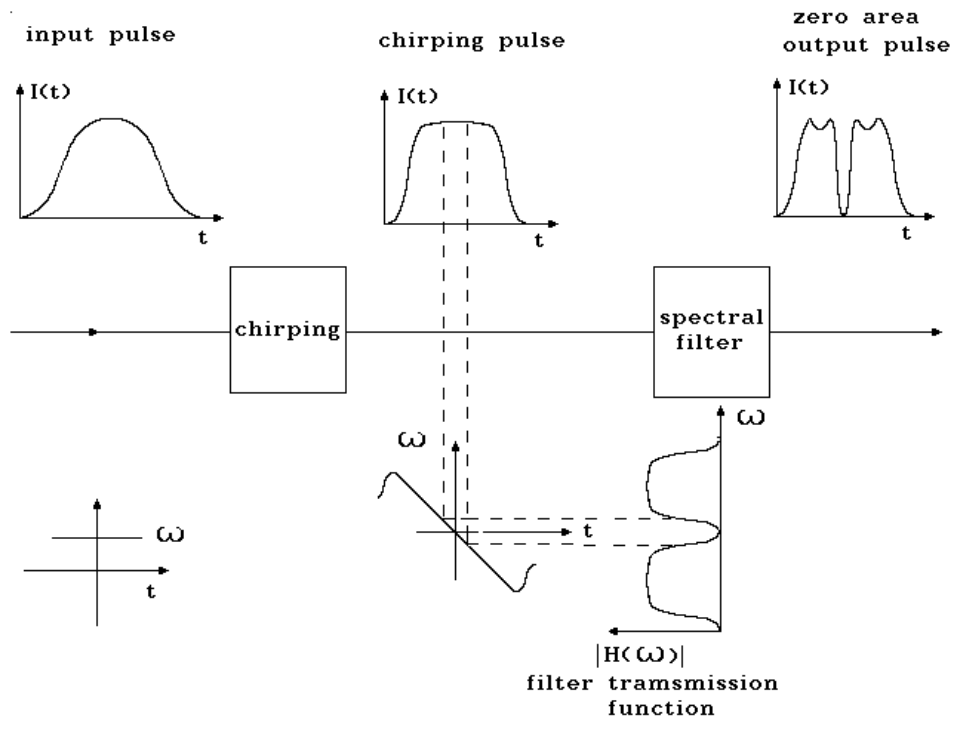
Fig. 2. Sketch of zero area pulse synthesation through self-phase modulation and spectral filtering

tical pulse produced by the shaping system is amplified up to the saturation level in the second undulator. Large energy spread is induced in the significant

3
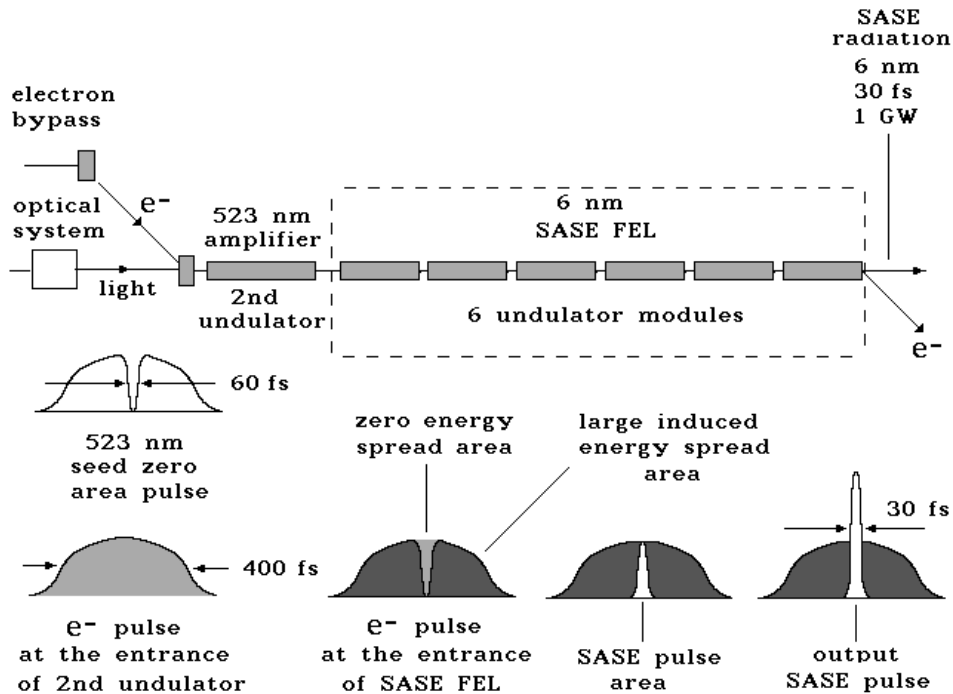
Fig. 3. Schematic diagram of zero area pulse technique for the generation of the soft X-ray femtosecond SASE pulses

fraction of the electron beam due to the FEL interaction process, and only a small part of the electron bunch (near the center of the zero area light pulse) is capable to produce radiation in the 6 nm SASE FEL (see Fig. 3).

The SASE FEL described in this paper will provide soft X-ray pulses with 30 fs (FWHM) duration. On the basis of the TTF parameters it should be possible to achieve an average brilliance of 10^{22} photons s^{-1}mrad^{-2}mm^{-2} per 0.1% BW. The average number of photons can exceed 10^{12} photon/pulse. Present conceptual design is compatible with the layout of the soft X-ray SASE FEL being under construction at DESY and can be realized with minimal additional efforts.

Specific realization of the proposed femtosecond SASE FEL scheme makes use of and is compatible with existent facility at the TESLA Test Facility. The goal of the TTF FEL is to reach SASE FEL saturation in the soft X-ray range with six undulator modules, and in the second phase to built fully co-herent soft X-ray FEL facility based on an idea of a self-seeding option [3,4]. The X-ray self-seeding scheme consists of two undulators (four and six mod-ules, respectively) and an electron bypass and X-ray monochromator located between them. Figures 1 and 3 illustrate how the proposed facility for "manip-ulating" the energy spread along the electron bunch fits the TTF FEL layout. The first stage of 523 nm FEL amplifier is placed before electron beam bypass. The optical shaping system can be mounted in the optical path foreseen for the installation of the X-ray monochromator. The second undulator is placed

4

after the electron beam bypass. It is important to stress that the requirements for bypass in our case are very close (practically identically) to those for the electron bypass in the two-stage soft X-ray SASE FEL which is presently under construction. The seeding 523 nm laser required for femtosecond X-ray FEL option is a simple and cheap extension of the existent photoinjector laser facility.

The paper proceeds as follows. In section 2 we outline the scope of the research associated with the femtosecond soft X-ray source. In section 3 we describe the basic ideas of the proposal. Section 4 describes two-stage 523 nm FEL amplifier used for preparation of the electron pulse with zero are energy spread in the center of the electron beam. Soft X-ray SASE FEL is described in section 5. Optimization of the parameters of the FEL amplifiers has been performed with three-dimensional, time-dependent FEL simulation code FAST [5] taking into account diffraction effects, space charge field, energy spread effects, arbitrary axial and transverse profile of the electron bunch, the effects of finite optical pulse duration and nonlinear effects. Section 6 deals with description of optical elements, in particular, the seed zero area optical pulse system and the energy spread shaping technique. Finally, in section 7 we describe electron bypass separating the stages of the 523 nm FEL amplifier. The functions of the electron bypass consist in making the time delays of the electron and the light beams equal, and in suppressing the modulation of the electron bunch produced in the first undulator.

2   Scientific opportunities with the femtosecond soft X-ray SASE FEL

To date, the study of ultrafast dynamics in the field of physics, chemistry, and biology has relied largely on femtosecond optical pulses in the visible or infrared spectral range. Using fs optical lasers researches could collected a wealth on information on the details of reaction pathways in many molecular systems e.g. J_2, CH_2J_2, and even larger systems [6]. The importance of the field is underlined by awarding the Nobel Prize in chemistry to A. Zewail. Since all information in optical fs-experiments is obtained from spectroscopic results, e.g. ionization probability or kinetic energy of photoelectrons, a detailed knowledge on the involved - sometimes rather complex - energy surface is required for the interpretation and understanding of the experimental data. Soft X-rays have several advantages compared to optical light pulse. Thanks to the element specific absorption of inner shell electrons well-defined atoms can be excited selectively [7]. Moreover, chemical bonds can be selected by their well-known chemical shift, e.g. in inner shell photoelectron spectra (XPS) [8]. The latter can be used in order to identify surface and bulk states of condensed matter. Finally, the local excitation of tightly bound core levels allows the determination of structural information with various techniques (EXAFS,

XANES, and photoelectron diffraction). Therefore, fs soft X-ray pulses hold great promises for new and exciting experiments in many fields of research which will give deep insight into the dynamics of nuclei and electrons on the time scale of vibrational motion.

The vibrational period of nuclear motion depends on the strength of chemical bonds and the mass of nuclei. In heavy molecules like J_2 the period is approximately 100-200 fs while for light molecules, especially hydrogen containing molecules it last about 10-50 fs [9]. It is thus obvious, that the proposed new design for a soft X-ray FEL with 30 fs long pulses will have a considerable advantage compared to other proposed schemes [10,2] – some are already under construction or have emitted first light [11] - since their pulse duration of 200-300 fs is just at the limit for the studies on nuclear motion and lattice vibrations. Pump probe techniques which are commonly used with optical lasers, are highly desirable in order to make full use of the short pulses. Since precise timing is needed with a jitter of less than 30 fs we suggest to combine the proposed fs soft X-ray FEL with UV optical pulses generated in an additional undulator using the same electron beam as outlined in ref. [12].

Time resolved experiments with 30 fs resolution will open new scientific opportunities in chemistry, molecular physics, solid state physics and surface science. The use of pump-probe techniques will allow the study of vibrational and bond breaking and dissociation in complex molecules with element selectivity. Thanks to the local excitation it will be possible to distinguish the vibrational motion of non-equivalent atoms, e.g. the central and the terminal nitrogen atom in N_2O. Moreover, time resolved photoemission (XPS) can be used to ascertain decay rates and vibrational periods in well-defined subgroups in large molecules, since the chemical shift in the XPS spectrum is a fingerprint of chemical bonds.

In a similar way, research on clusters and nanocrystals will benefit from the proposed FEL. As a result of their small size a large fraction of atoms are located at the surface [13]. Time resolved studies (pump-probe) will allow the investigation of surface and bulk states separately. Furthermore, photon induced reactions, phase transitions and electron transfer processes can be studied on a time scale of a few ten fs. Photoelectron, ion and fluorescence signals as well as combinations (electron ion: PEPICO, ion-ion, PIPICO, for the study of fragmentation and dissociation) can be used as a monitor. Metal, semiconductor and covalently bound systems, and complexes that play an important role in atmospheric processes are great interest in this context.

The element specific excitation of soft X-rays will allow the study of photodynamical processes of individual atoms and molecules on surfaces. Time resolved EXAFS/XANES or photoelectron diffraction making use of two colour pump- and probe techniques will give information on the motion (vibration dissociation) on well characterized surfaces in real time. The reaction dynamics of adsorbates is of major importance for the understanding of chemical

processes at surfaces and an important issue in this context. Catalytic reactions of metal and semiconductor interfaces are of particular interest. UV light can induce a chemical reaction like oxidation, which can be studied by looking at reaction products on a fs time scale. The high photon density of the FEL beam - especially when focussed into a small spot - will result in efficient photodesorption and plasma formation. Many processes occurring in laser induced plasma going on in the plume are not well understood. Detailed information can be obtained using two-colour pump probe experiments and detecting photoelectrons and ions ejected from the plasma plume. Photoreactions and phase transition in bulk samples can be investigated with time resolved X-ray emission spectroscopy. The mean free path length of soft X-rays is much larger than the internuclear separations in solids. Thus, time resolved studies of bulk properties, the dynamics of atoms doped into solids and photoinduced reactions at buried interfaces become feasible.

All applications outlined above are based on 30 fs long soft X-ray pulses. One can expect that first successful experiments in this field will stimulate further applications.

3 General description of femtosecond X-ray FEL at the TESLA Test Facility

Present design assumes to use project parameters of the TESLA Test Facility accelerator [2] (see Table 1). Facility for production of femtosecond SASE X-ray pulses consists of a two-stage seeding system operating at the wavelength of 523 nm. Figure 1 shows a schematic diagram of a seed system for the femtosecond soft X-ray SASE FEL at the TESLA Test Facility. The scheme consists of seed quantum laser, two undulators and optical pulse shaping system located between them. The first undulator operates in a linear regime and produces short light pulse (of about 300 fs duration) synchronized with the electron bunch. After the exit of the first undulator the electrons are guided through a bypass and the radiation enters the shaping system. A zero area light pulse with peak power of about 10 kW is generated by pulse shaping system (see Fig 2). This radiation pulse is amplified up to the saturation level in the second undulator. At the exit of the second undulator the most fraction of the electron bunch has large energy spread due to the FEL process except of a small region in the center of zero pulse area. This of the essence of the energy spread shaping technique. The process of amplification of radiation in the X-ray undulator develops in the same way as in conventional SASE FEL: fluctuations of the electron beam current density serve as the input signal. The seeding radiation (523 nm wavelength) does not interact with the electron beam in the X-ray undulator and is diffracted out of the electron beam. Since the gain of the FEL amplifier is very sensitive to the energy spread, only this small part of the electron bunch produces the radiation, thus provid-

7

Table 1
Parameters of the electron beam at the TESLA Test Facility accelerator

Energy	1000 MeV
Bunch charge	1 nC
rms bunch length	50 μm
Normalized rms emittance	2π mm mrad
rms energy spread	0.1 %
Number of bunches per train	7200
Repetition rate	10 Hz

ing short pulse duration (see Fig. 3). For ultrashort zero area of seed optical field, the slippage of radiation with respect to the electron bunch in the 523 nm high-gain FEL amplifier can be an essential mechanism for shortening the SASE radiation pulse. Starting with zero area of optical field of 60 fs duration (FWHM) we can obtain 30 fs (FWHM) pulses at the wavelength of 6 nm.

An attractive feature of this scheme is the absence of no apparent limitations which would prevent operation at even SASE pulse with duration close to coherence time (about 2 fs in our case). For example close to end of 523 nm FEL operation (i.e. close to saturation) we can use a magnetic delay to position the 523 nm radiation near the tail end of undisturbed part of the bunch. An experimenter can easily control the duration of "zero" area by tuning the magnetic field in the shifter (a three-dipole chicane). In this technique we use zero are of seed optical field that is much longer than the produced soft X-ray SASE pulse.

4   523 nm two-stage FEL amplifier

4.1   First stage of 523 nm amplifier

The function of the first stage of 523 nm FEL amplifier is to prepare short optical pulse strictly synchronized with the electron bunch. The amplifier is seeded by the laser pulse of 10 ps pulse duration and 30 kW peak power. The duration of the seeding pulse is much larger than the electron pulse time jitter of ± 1 ps, so it can be easily synchronized with the electron bunch.

The parameters of the first stage of the 523 nm FEL amplifier are presented in Table 2. It operates in a linear regime with a power gain $G \simeq 2$. This value is much less than the power gain at saturation, $G_{\text{sat}} \simeq 10^6$ (at input power $W_{\text{in}} \simeq 30$ kW). At such a choice of the power gain in the first stage the energy spread induced by the FEL process amounts to $\Delta E/E \simeq 10^{-5}$, and is much less than the initial energy spread ($\Delta E/E \simeq 10^{-3}$) in the beam.

The first stage of FEL amplifier consists of two planar undulator sections placed in crossed positions, as it is illustrated schematically in Fig. 4. Both

Table 2
Parameters of two-stage 523 nm FEL amplifier at the TESLA Test Facility at DESY

Undulator
Type	Planar
Period	7.5 cm
Peak magnetic field	1.47 T
External β-function	300 cm
First stage:	
Length of x-polarized undulator	1.35 m
Length of y-polarized undulator	1.2 m
Second stage:	
Length of undulator	8.25 m

Radiation
Wavelength	523 nm
Input radiation peak power	30 kW
Duration of seeding pulse (FWHM)	10 ps
Output radiation peak power	60 kW
Duration of output pulse (FWHM)	300 fs
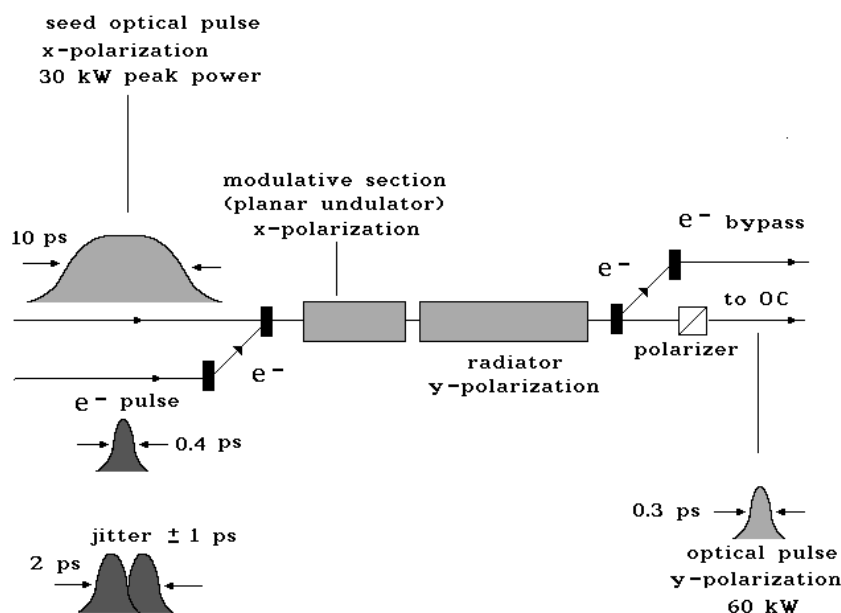
Fig. 4. Schematic illustration of design configuration for the first stage of 523 nm FEL amplifier

undulator sections have the same period and field strength. The 523 nm x-polarized seed radiation with 30 kW peak power and electron beam enter the first undulator section, which is used to modulate the electron beam. Passing the first undulator section the beam and seed radiation enter the second undulator section which is rotated by 90° relative to the first undulator section. The x-polarized seed radiation does not interact with the electron beam and thus propagates freely. However, a new y-polarized radiation component is generated by the density-modulated electron beam and rapidly reaches 60
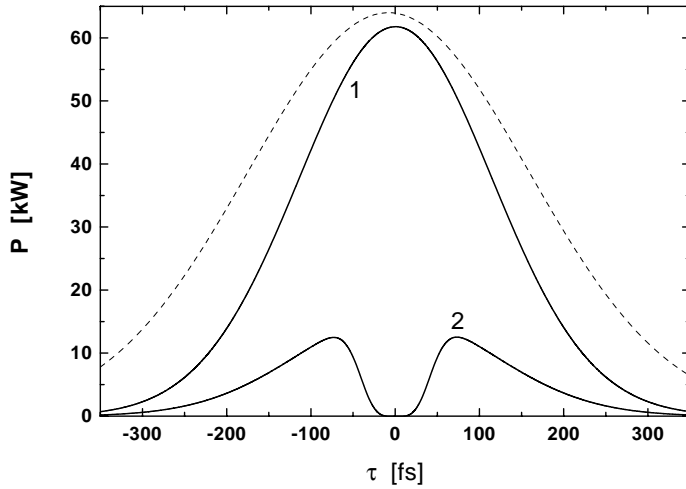
Fig. 5. Temporal profile of the radiation pulse at the exit of the first stage of 523 nm FEL amplifier (curve 1). Curve 2 present temporal profile of the radiation pulse after optical pulse shaping system. Dotted line denotes current profile of the electron bunch.

kW level peak power. Then the electron and the light beam are separated. The electron beam is guided through a nonisochronous bypass and the radiation enters the polarizer which selects y-polarization. The radiation pulse after polarizer has short duration and is synchronized with the electron bunch (see Fig. 5). Finally, the radiation pulse is directed to the optical pulse shaping system. Details of the optical pulse shaping system are presented in section 6.

4.2   Second stage of 523 nm two stage FEL amplifier

The function of the second stage of 523 nm two-stage FEL amplifier is to prepare electron bunch with prescribed energy spread distribution along the electron bunch. Parameters of the second stage of the 523 nm FEL amplifier are presented in Table 2. The input signal for the second stage comes from optical pulse shaping system. It has appearance of zero area pulse (see Fig. 5). Main physical effects influencing the operation of the 523 nm FEL amplifier are the diffraction, space charge and slippage effects. The required level of the energy spread in the FEL amplifier is induced only in the nonlinear stage of the FEL amplifier operation when the electrons become to lose visible fraction of their energy. In order to reach nonlinear stage, the undulator should be sufficiently long (see Fig. 6). Optimized length of the undulator is equal to 8.3 m, i.e. 110 undulator periods. Slippage effect at this distance play visible role in formation of the radiation, despite kinematic slippage (of about 60 microns) is visibly suppressed, by a factor of four, due to decrease of the group velocity of the radiation interacting with the electron beam [14]. This effect explains significant difference between the shape of the seeding pulse (see Figs. 5 and 7) and radiation profile and induced energy spread in the

10
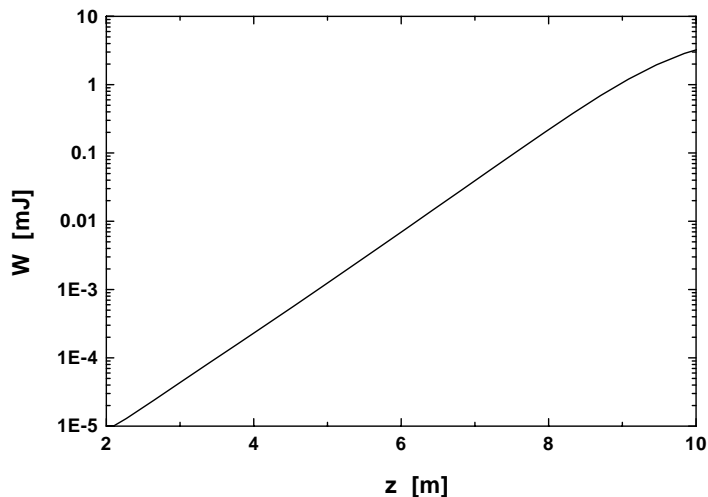
Fig. 6. Energy in the radiation pulse versus the length of the undulator of the second stage of 523 nm FEL amplifier.
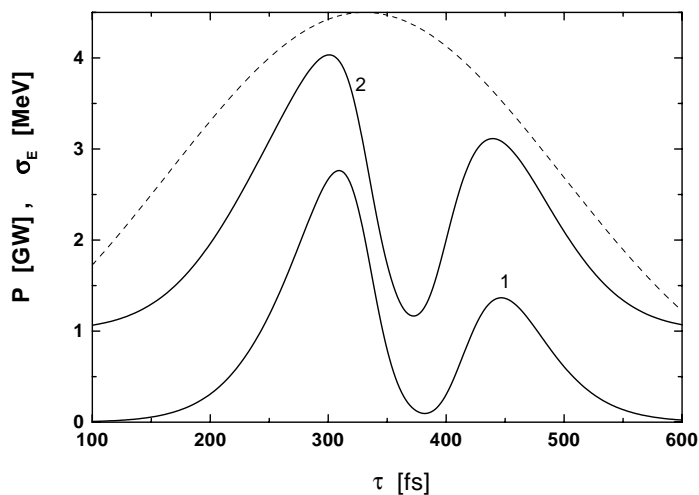
Fig. 7. Temporal profile of the output radiation (curve 1) and energy spread in the electron bunch (curve 2) at the exit of 523 nm FEL. Dashed line denotes current profile of the electron bunch.

electron beam at the undulator exit.

A dispersion section is installed at the exit of the second stage of 523 nm FEL amplifier in order to provide more homogeneous distribution of the electrons in the phase at the entrance to the X-ray undulator. A simple chicane consisting of three dipoles with $R_{56} = 0.5$ mm is sufficient for this purpose.

5 Femtosecond X-ray SASE FEL

X-ray undulator follows immediately after the second stage of the two-stage 523 nm FEL amplifier (see Fig. 3). The process of amplification of radiation in

Table 3

Parameters of femtosecond X-ray FEL at the TESLA Test Facility at DESY

Undulator	
Type	Planar
Period	2.73 cm
Peak magnetic field	0.497 T
External β-function	300 cm
Length of undulator	26 m
Radiation	
Wavelength	6.4 nm
Bandwidth, $\Delta\lambda/\lambda$	0.5%
rms angular divergence	15 μrad
rms spot size at the undulator exit	90 μm
Pulse duration (FWHM)	30 fs
Power average over pulse	2 GW
Flash energy	50 μJ
Average power	4 W
Peak spectral brilliance	3×10^{30} Phot./(sec$\times$ mrad$^2 \times$mm$^2 \times$ 0.1 % bandw.)
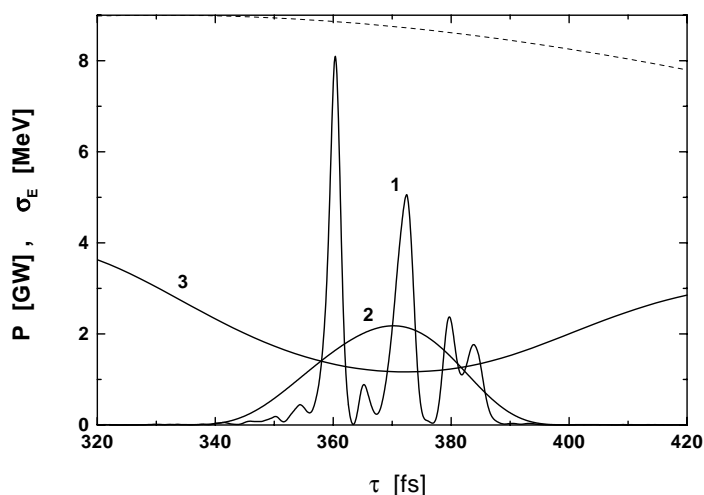
Fig. 8. Temporal structure of the output radiation from femtosecond X-ray FEL. Curve 1 corresponds to the single shot, and curve 2 is the averaged value. Curve 3 represent the energy spread along the electron bunch at the undulator entrance. Dashed line denotes current profile of the electron bunch.

the X-ray undulator develops in the same way as in conventional SASE FEL: fluctuations of the electron beam current density serve as the input signal. The seeding radiation (523 nm wavelength) does not interact with the electron beam in the X-ray undulator and is diffracted out of the electron beam. Since the gain of the FEL amplifier is very sensitive to the energy spread, only this small part of the electron bunch produces the radiation, thus providing short pulse duration. Parameters of the femtosecond X-ray FEL amplifier are

presented in Table 3. The only difference in parameters from the main option of the TTF FEL [2] is that the FWHM pulse duration is reduced down to the value of 30 fs. Figure 8 represents temporal structure of the radiation pulse at the exit of the X-ray FEL at the undulator length 26 m.

6   Optical system

6.1   The seed quantum laser system

Figure 9 shows schematic layout of the seed laser system for femtosecond SASE FEL integrated into the present laser system of TTF photoinjector. Present laser facility is marked with the dashed borders in the figure. The seed laser for femtosecond FEL is simple and cheap extension of the existent laser facility. An upgrade assumes installation of an outcoupling mirror after pulse pickers (see Fig. 9). This mirror is semi-transparent and approximately 10% of the radiation power (or about 100 nJ energy of pulse) is reflected and delivered to the seed laser system. One single pass amplifier is foreseen to amplify the outcoupling pulses up to about 1 μJ. The amplifier for stability reasons will be diode-pumped. The non-linear crystal, KDP, will provide 2nd harmonic (523 nm). The conversion to the higher harmonic leads to a pulse shortening from 8 to 5 ps. A pulse-stretcher is foreseen, because longitudinally flat-top pulses longer then 5 ps are required.

The peak power of the amplifier, 30 kW, significantly exceeds the value
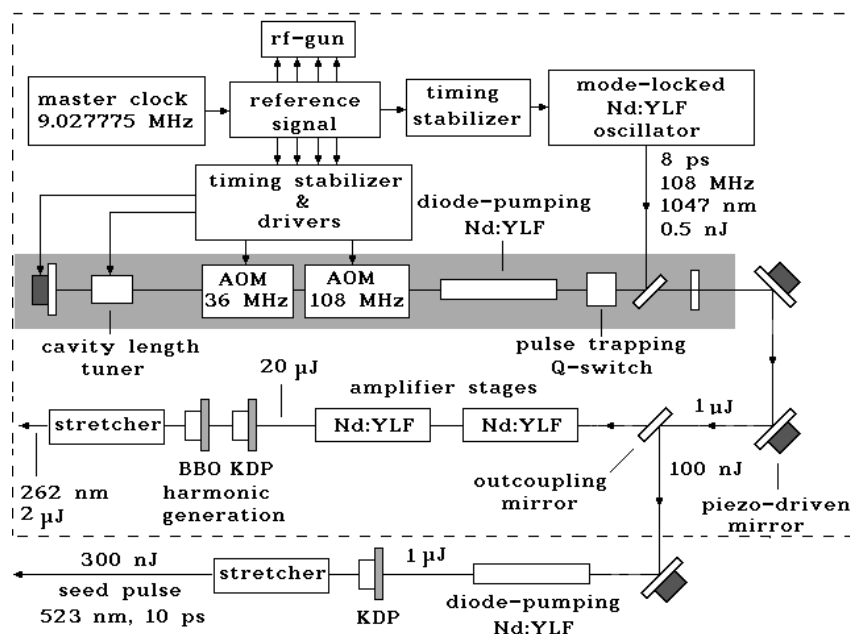
Fig. 9. Schematic layout of the proposed picosecond seed laser system for femtosecond FEL at TTF. The dashed borders denote the existent TTF laser facility

13

of 30 W — the effective power of shot noise in the electron beam at the undulator entrance. The average output power of the amplifier is by an order of magnitude less than output power of the existent laser for the photoinjector. The problem of synchronization of the electron and laser pulses is naturally solved, because the photoinjector and the seed laser use the common master oscillator and timing system. Laser control used by TTF has demonstrated stability at the level we require, namely $\pm 2\%$ pulse to pulse in the energy and ± 1 ps in phase.

6.2 Shaping through spectral filtering

Optical pulse shaping is performed in a two-step process sketched in Fig. 2 [16]. In the first step a phase modulation is impressed on the pulse by self-phase modulation in a nonlinear refractive index material. The transformed pulse is spectrally broadened, or in time domain, a chirped pulse. The refractive index of many materials depends nonlinearly on the radiation field intensity. Usually the lowest order of this dependence is expressed as $n = n_0 + n_2 I(t)$, where $I(t)$ is temporal intensity profile. Progress in the technology of high-quality monomode optical fibers supplied the desired equipment for producing ultra broadband radiation with a linear frequency chirp (see Fig. 10). The main advantage of the fiber is the possibility of retaining a small cross section of the optical beam propagating over a long distance.

The propagation of optical pulses in single-mode fibers is affected by dispersion and n_2 (often referred to as "Kerr type" nonlinearity). For their characterization we introduce a dispersion length $L_D = \tau_0^2/k''$ and nonlinear interaction length $L_{NL} = (\gamma_2 I)^{-1}$, where τ_0 is the FWHM of the input pulse, $k'' = d(v_g^{-1})/d\omega$ is the group velocity dispersion parameter, v_g is the group velocity, and $\gamma_2 = n_2\omega_0/c$. For fused silica ($k'' \simeq 6 \times 10^{-26}$ s^2/m, $n_2 \simeq 3.2 \times 10^{-16}$ cm^2/W), an affective fiber area of 10 μm^2, $W = 30$ kW, $\tau_0 = 300$ fs, and $\lambda = 523$ nm corresponds to $L_D \simeq 1.6$ m and $L_{NL} \simeq 1$ mm [16]. A practical limit for the maximal power W that can pass through the fiber is defined by
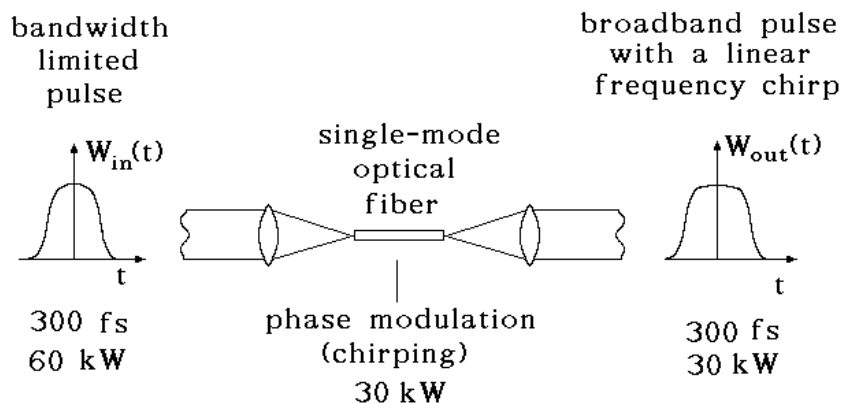
Fig. 10. Sketch of optical pulse chirping

damage threshold. Typical damage intensities in the case of sub-picosecond pulses are in the order of $\mu J/\mu m^2$ [16]. In our case the intensity in the optical fiber is about one $nJ/\mu m^2$, and is by three orders of magnitude less than the damage threshold.

Let us discuss the problem of optimization of the optical fiber length. In the optical fiber pulse propagates with the group velocity $v_g = c/n$ (the refractive index is $n = 1.46$ for fused silica). The choice of the fiber length is based predominantly on the group delay effect. We select the fiber with the length of $L \simeq 1$ cm. Calculation shows that in this case the ratio of the spectral bandwidth before ($\Delta\omega_{in}$) and after ($\Delta\omega_{out}$) the fiber reaches a value of about $\Delta\omega_{out}/\Delta\omega_{in} \simeq 8$. The chirped pulse bandwidth is clearly limited by the bandwidth of 523 nm FEL amplifier $\Delta\omega_{amp}/\omega \simeq 3\%$, and is very close to $\Delta\omega_{out}/\omega \simeq 3.5\%$. Chirping the optical pulse in the fiber has to be done to avoid stimulated Raman scattering (SRS) effect. The SRS effect starts from spontaneous emission and grows exponentially along the optical fiber. In the high-gain limit we can write an asymptotic expression for intensity of SRS signal: $I_R(z) = I_R(0)\exp(G_R z)$, where $I_R(0)$ is spontaneous emission intensity. The grows rate, G_R, is proportional to the pump intensity I (i.e. intensity of chirping pulse), and is given by the expression $G_R = gI$. For fused silica at 500 nm wavelength the gain coefficient is $g \simeq 2 \times 10^{-11}$ cm/W. SRS effects can be neglected for the optical fiber length, $L < L_{th} \simeq 16/(gI)$. In our case ratio L/L_{th} is about 0.3, and the SRC signal is by 5 order of magnitude smaller with respect to the saturation level. Thus, we find that the SRS effects are not important in our case.

The second step of preparation optical pulse is the shaping through filtering. A shaping technique best suited for the sub-picosecond pulses consists of "manipulating" the pulse spectrum in amplitude and phase [16]. The pulse to be shaped is spectrally dispersed using grating. The spectrum is propagated through a mask which spectrally filters the pulse. The spectral components are recollimated into a beam by a second grating. Figure 11a shows a setup for spectral filtering in a dispersion-free grating-lens combination. Each spectral component is focused at the position of the mask. Since, to a good approximation, the frequency varies linearly in the focal plane of the lens, a variation of the complex transmission across the mask causes a transfer function of the form: $H(\omega) = R(\omega)\exp[-i\,\psi(\omega)]$, where $R(\omega)$ represents the amplitude transmission and $\psi(\omega)$ the phase change experienced by a spectral component at frequency ω. These masks can be produced by microlithographic techniques. A pure phase filter, for example, could consist of a transparent material of variable thickness. If we neglect the effects caused by the finite resolution, the field at the device output is: $\bar{E}_{out}(\omega) = \bar{E}_{in}(\omega)R(\omega)\exp[-i\,\psi(\omega)]$, and $\bar{E}_{out}$ is the field spectrum of the input pulse. The mask can be sequence of an amplitude-only and phase-only filter to generate the desired $H(\omega)$. Many different output fields can be realized by using different mask functions. Of course, the shortest temporal structures that can be obtained are limited by the finite width of the

(a)
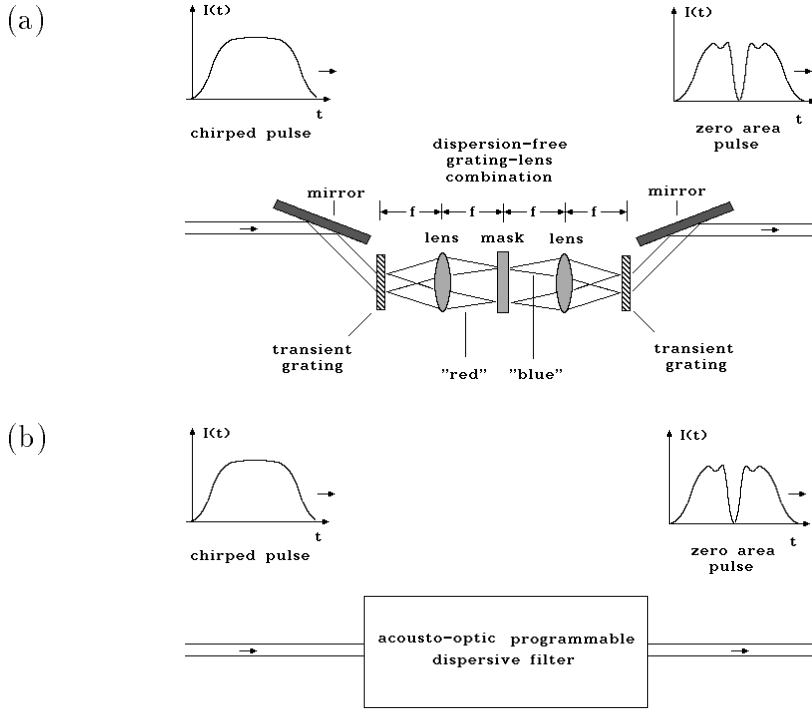
Fig. 11. Spectral filtering in a dispersion-free grating-lens combination (upper drawing) and in an acousto-optic programmable dispersive filter (lower drawing)

input pulse spectrum. The narrowest spectral features that can be impressed on the spectrum are determined by the grating dispersion, mask structure, and size of the focal spot.

An interesting possible alternative to the dispersion-free grating-lens combination could be an acousto-optic programmable dispersive filter (AOPDF) proposed in [17], a device commercially available today (see Fig. 11b). The acoustic wave is generated in the TeO_2 crystal by a piezoelectric transducer. The transducer has a bandwidth larger than 20 MHz, which translates into an optical bandwidth of 150 THz; the associated temporal resolution is then about 7 fs. The acoustic power is limited to 4 W, which results in a maximum diffraction efficiency of 30%. The filter has a large group-delay range that extends over 3 ps [18].

6.3 Optical elements

The optical system needed for femtosecond soft X-ray SASE FEL has to satisfy two requirements. First, it has to produce 300 fs light pulses with zero area of 60 fs duration. Second, the output pulse must fully overlap the electron bunch at the entrance to the second stage of 523 nm FEL amplifier, i.e. the optical path length must be exactly the same as that of the electron bunch going through the bypass of the TTF with extra path length of 12 mm. These basic requirements define all the details of the optical system. A sapphire spherical
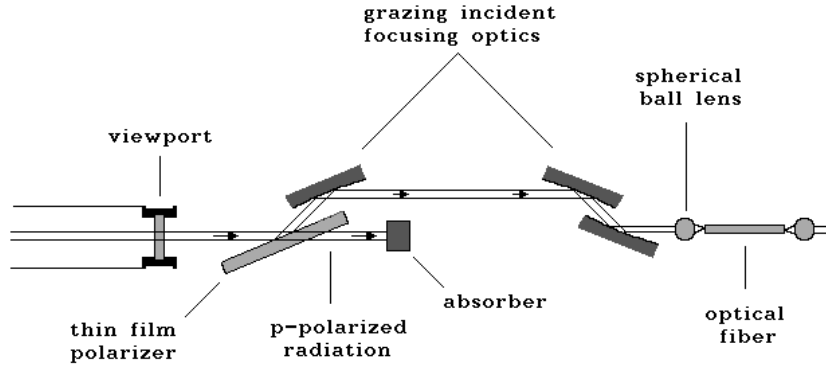
Fig. 12. Schematic layout of a light beam filter based on thin film polarizer. P-polarized light is transmitted, while s-polarized light, which naturally synchronized with electron bunch, is reflected. The extinction ratio is 100:1
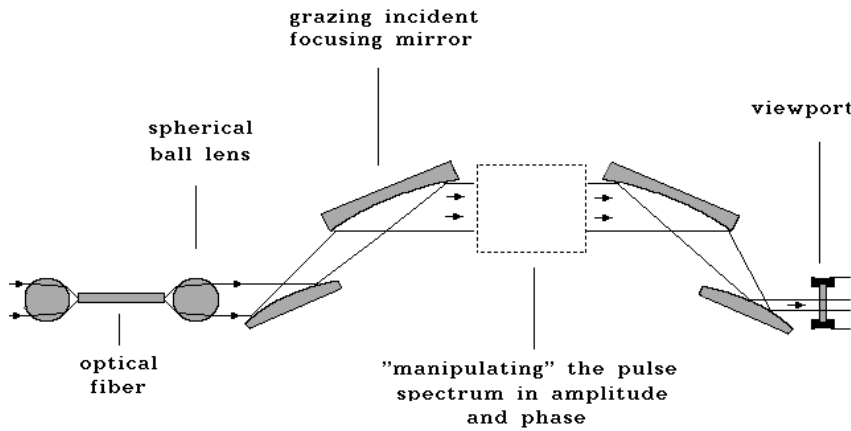
Fig. 13. Optical arrangement for focusing system

ball micro lenses (0.25 mm diameter, numerical aperture NA > 0.4) has been chosen for our design as a microscope objective and end-fiber lens. Figure 12 shows setup for the polarizer. The input pulse is focused on a thin film polarizer. After reflection, the s-polarized pulse is focused in a microscope objective and p-polarized pulse is sent through the polarizer where it is absorbed. When polarizer is mounted at Brewster's angle (60°), extinction ratio exceeds 100:1. In this design we have only about 1 mm extra pulse length for the optical beam. For minimum delay, pre-microscope objective focusing optics and pre- and post-spectral filtering optics are grazing incident, high-reflectivity mirrors (see Figs. 12 and 13). The function of the pre- and post-focusing optics is twofold: i) to demagnify and magnify the source as required, and ii) to bring the beam along the center of the second undulator. For maximum flexibility we assume to install optical shaping system into atmosphere. An entrance and exit windows of appropriate material (sapphire, 12 mm diameter, 1.5 mm thickness) separates the vacuum from the optical elements.

17

7 Electron bypass

The electron bypass has to deflect the electron beam out of the straight flight pass to make room for the optical elements. In addition the microbunching introduced in the electron bunch in the first undulator has to be removed without increasing the overall length of the bunch significantly. The electron optical functions at the exit of 1st undulator and the entrance of the 2nd undulator are determined by the undulators and have to be matched by the bypass electron optics.

We calculate the evolution of the beam modulation in the bypass within the one-dimensional approximation. The phase space distribution of the particles is described by means of the distribution function $f(P, \psi, z)$ written in "energy-phase" variables $P = (E - E_0)$ and $\psi = k_w z + \omega(z/c - t)$, where E_0 is nominal energy of the particles, $k_w = 2\pi/\lambda_w$ is the undulator wavenumber and ω is the frequency of radiation.

In the linear approximation the distribution function of the modulated electron beam at the entry of the bypass can be represented as $f(P, \psi) = f_0(P) + f(P, \psi)_{in}$, where

$$f(P, \psi)_{in} = \frac{a_1}{2} f_0(P) \exp(-i\,\psi) + \text{C.C.}$$

When the energy spread in the electron beam is Gaussian the distribution has the form

$$f_0(P) = \frac{1}{\sqrt{2\pi \langle (\Delta E)^2 \rangle}} \exp\left(-\frac{(E - E_0)^2}{2\langle (\Delta E)^2 \rangle}\right) \ .$$

Here $\sqrt{\langle (\Delta E)^2 \rangle}$ is the standard deviation. Integration of the distribution function over energy provides the distribution of the beam density modulation:

$$\int_{-\infty}^{\infty} f(P, \psi)_{in}\, d P = a_1 \cos(\psi) \ .$$

It is seen from this expression that at the entrance into the bypass the electron bunch is modulated in density with the wavenumber $k = k_w + \omega/c$. As $k_w \ll \omega/c$, the bunch modulation wavelength is almost identical to the radiation wavelength.

When an electron with relative energy offset P passes the bypass, its phase shifts with respect to an electron with nominal energy by

$$\Delta\psi = \psi(P) - \psi(0) = R_{56}\frac{\omega P}{c E_0} \ ,$$

where R_{56} is the (5,6) element in the linear transfer matrix of bypass. As a

result, one obtains the following expression for the distribution function at the exit of the bypass:

$$f(P, \psi)_{\text{out}} = \frac{a_1}{2} f_0(P) \exp[-\mathrm{i}\,\psi - \mathrm{i}\,\Delta\psi(P)] + \text{C.C.} ,$$

which corresponds to a distribution of particles in real space given by:

$$\frac{a_1}{2} \exp(-\mathrm{i}\,\psi) \int\limits_{-\infty}^{\infty} \mathrm{d}\,P f_0(P) \exp[-\mathrm{i}\,R_{56}\omega P/(cE_0)] + \text{C.C.}$$

Electron beam from a linear accelerator have often energy distribution of from between a Gaussian and parabolic profile. For the specific case of a Gaussian and parabolic profile the density modulation of the beam at the exit of bypass have the form

Gaussian energy distribution:

$$\exp[-\langle(\Delta E)^2\rangle R_{56}^2\omega^2/(2c^2 E_0^2)]a_1\cos(\psi) ,$$

Parabolic energy distribution with energy interval $(E_0 - \Delta E, E_0 + \Delta E)$:

$$\frac{\cos[\Delta E R_{56}\omega/(cE_0)]}{[\Delta E R_{56}\omega/(cE_0)]^2}3a_1\cos(\psi) \qquad \text{for} \quad \Delta E R_{56}\omega/(cE_0) \gg 1 .$$

It should be noticed that at the exit of the first undulator the electron beam is modulated also in the electron velocities. It can be shown that this velocity modulation is suppressed to the same degree as the density modulation.

Therefore, we can expect that the problem of suppressing the beam modulation induced in the 1st stage of the 523 nm FEL amplifier can be solved quite naturally due to the presence of the energy spread in the electron beam. Parameters in our case are:

$$\sqrt{\langle(\Delta E)^2\rangle}R_{56}/E_0 \simeq 2.5\mu\text{m} , \quad \lambda = 2\pi c/\omega = 0.5\mu\text{m} .$$

This leads to the suppression of the electron beam modulation by a factor of S. The details of the energy distribution may influence the factor S. In practical situation $\exp(-2000) \ll S \ll 3 \times 10^{-3}$. The first stage of 523 nm FEL amplifier operates in a linear regime with output power $W_1 \simeq 60$ kW. This value is by 10^6 times less than the power at saturation ($W_{\text{sat}} \simeq 30$ GW). At such choice of the power gain in the first stage the amplitude of the first harmonic of the beam density modulation induced by the FEL process is about $a_1 \simeq \sqrt{W_1/W_{\text{sat}}} \simeq 10^{-3}$. On the other hand amplitude of the first harmonic of the shot noise beam density modulation at the entrance to the second stage is about $a_1^{(\text{sh})} \simeq \sqrt{W_{\text{sh}}/W_{\text{sat}}} \simeq 10^{-5}$. As a result, $Sa_1 \ll a_1^{(\text{sh})}$, and the initial modulation of the electron beam at the entrance into the second stage is given by the shot noise only.

Table 4
Parameters of the electron bypass

Main bypass	
Length	21 m
Extra path length	12.4 mm
Max. distance to the straight path	23.6 cm
Dipole bending angle	52.4 mrad
Extra path length for electrons with 0.1% energy deviation	0.73 μm
Tuning bypass	
Length of tuning bypass	4.8 m
Tunability of path length	0-0.952 mm
Max. distance to large bypass	43.6 mm
Tuning dipole bending angle	21.8 mrad
Extra path length for electrons with 0.1% energy deviation	0-1.86 μm
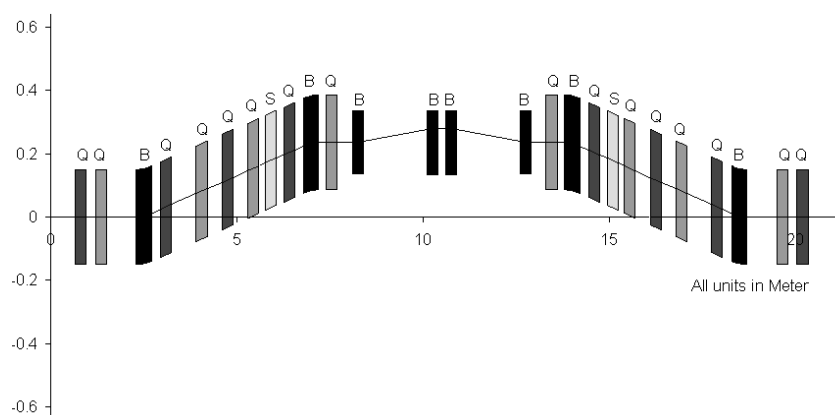
Fig. 14. Layout of the electron bypass. Here letters Q, S and B denote quadrupole, sextupole, and bending magnet, respectively.

The basic elements of the adopted symmetric bypass design are four dipole magnets. The first is located 1.3 m behind the first stage of 523 nm FEL amplifier and deflects the beam back in the direction parallel to the straight beam path at the distance of about 24 cm, which is sufficient for the installation of the optical elements. The total elongation of the electron beam path is approximately 12 mm. The layout of the bypass is shown in Fig. 14. In the middle of the bypass one finds a second mini-bypass, which serves for tuning the electron path length by up to 0.5 mm, i.e. approximately 10 times of the bunch length. The additional focusing and defocusing quadrupole magnets are needed to adopt the bypass electron optics to that in the undulator, for decoupling of the beampath elongation from the electron energy and for keeping the transverse beam cross section small enough. The bypass parameter list is presented in Table 4

Figure 15 shows the dispersion function as well as vertical and horizontal
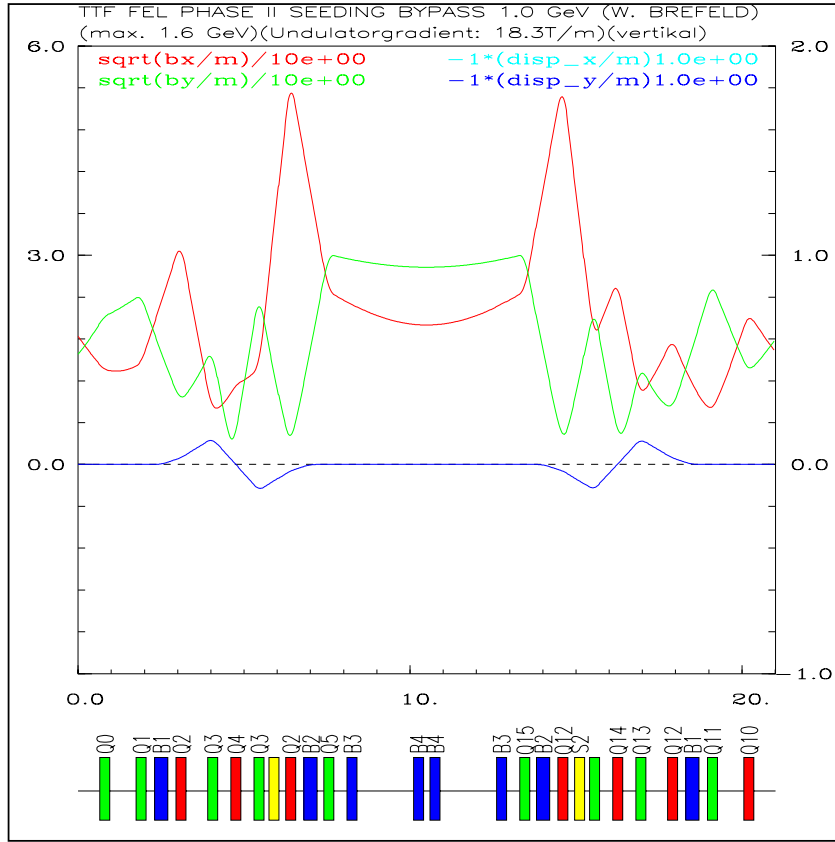
Fig. 15. Dispersion as well as vertical and horizontal beta-function along the bypass calculated for electron energy of 1 GeV
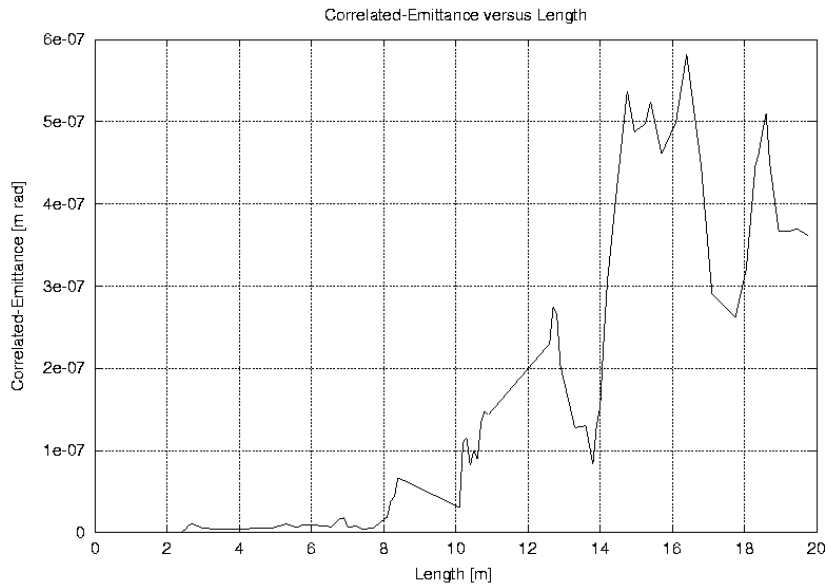
Fig. 16. CSR correlated-emittance increase across bypass at 1 GeV

beta functions along the bypass from which the cross section of the beam can be calculated using the known value of the beam emittance. Calculations have
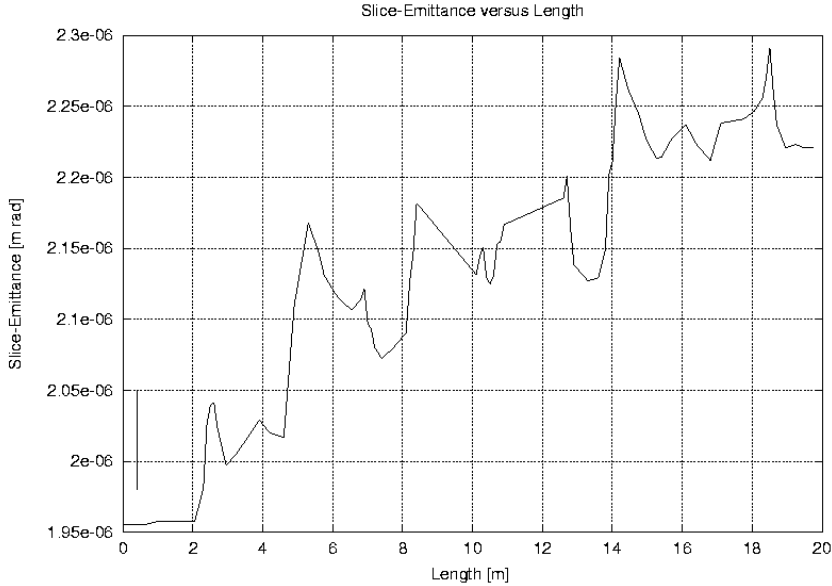
Fig. 17. CSR slice-emittance increase across bypass at 1 GeV

been made for 1000 MeV electron energy. In addition, one has to take into account that the energy spread of the electron beam will further increase the cross section. In order to decouple the energy-dependent path length elongation from the geometrical one a further focusing quadrupole magnet (Q3) has to be introduced between the two dipole magnets, which reduces back to small values the dispersion at the second dipole.

The transverse dimensions of the dipole and quadrupole magnets have been chosen such that they jut out in the direction of the straight beampath by no more than 15 cm. Preliminary optimization gives the length of the dipole and quadrupole magnets to be 20 cm and 30 cm, respectively. The final dimensions depend on the design of vacuum system.

The dispersion function shown in Fig. 15 has been calculated for the nominal energy of 1000 MeV. Due to the energy bend of about 0.1% effects of chromaticity could lead to an increase of the beam cross section at the end of the bypass. Therefore, bypass design foreseens installation of sextupole magnets in order to compensate chromaticity efects.

The mini-bypass located in the middle of bypass provides fine tuning of the effective path length up to 0.5 mm which reduces down to a realistic level the requirements for the alignment of the bypass and the optical shaping system elements. This bypass is 2.7 m long and consists of four dipole magnets of rectangular shape, 10 cm long which deflect the beam by up to 1.25°. The focusing of the beam over these 2.7 m is taken care of by quadrupole magnets of the main bypass, in addition such a bypass does not create dispersion at its end which one had to eliminate. Because there are no extra quadrupoles, there is also no possibility to correct for the energy dependent path elongation. However, the effect is less than one micron and is negligible.

22

For very short bunches, coherent synchrotron radiation (CSR) can dilute the horizontal emittance by similarly generated energy spread in the dipoles. Calculations of the CSR induced emittance dilution have been made using the DESY TRAFIC4 code [15] which includes field transients, bend-to-bend radiation, and radial forces. These results shows that the dilution of the slice emittance in the bypass is about 10% (see Figs. 16 and 17).

Acknowledgments

References

[1] R. W. Schoenlein et al., Science 287(2000)2237

[2] J. Rossbach, Nucl. Instrum. and Methods A 375(1996)269

[3] J. Feldhaus et al., Optics Communications 140(1997)341

[4] "Seeding Option for the VUV Free Electron Laser at DESY": Proposal. Available at DESY by request only

[5] E. L. Saldin, E. A. Schneidmiller, and M. V. Yurkov, Nucl. Instrum. and Methods A 429(1999)233

[6] L. Lehr et al., Science 284(1999)635

[7] J. Stöhr "NEXAFS Spectroscopy" (Springer, Berlin, 1992)

[8] W. Eberhardt "Applications of Synchrotron Radiation" (Springer, Berlin, 1995)

[9] E. Schreiber "Femtosecond Real-Time Spectroscopy of Small Molecules and Clusters" (Springer, Berlin, 1998)

[10] R. Tatchyn et al., Nucl. Instrum. and Methods A 375(1996)274

[11] J. Andruszkow et al., Phys. Rev. Lett. 85(2000)3825

[12] B. Faatz et al., DESY-print 00-94(2000)

[13] H. Haberland "Clusters of Atoms and Molecules" (Springer, Berlin, 1993)

[14] E.L. Saldin, E.A. Schneidmiller, and M.V. Yurkov, "The Physics of Free Electron Lasers" Springer-Verlag, Berlin, 1999

[15] M. Dohlus, A. Kabel, and T. Limberg, Nucl. Instrum. and Methods A 445(2000)84

[16] Jean-Claude Diels and Wolfgang Rudolph "Ultrashort Laser Pulse Phenomena" (Academic Press, San Diego-New York-Boston-London-Sydney-Tokyo-Toronto, 1996)

[17] P. Tournois, Opt. Commun. 140(1997)245

[18] F. Verluise et al., Optics Lett. 25(2000)575